Bias correction of Sentinel-2 with unmanned aerial vehicle multispectral data for use in monitoring walnut fruit forest in western Tien Shan, Kyrgyzstan

Erkin Isaev,* Maksim Kulikov, Evgenii Shibkov, and Roy C. Sidle
University of Central Asia, Mountain Societies Research Institute, Bishkek, Kyrgyzstan

Abstract. The scope of our work is to compare Sentinel-2 and unmanned aerial vehicles (UAV) imagery from Western Tian Shan for monitoring applications in walnut fruit forests. Because acquiring field data on walnut fruit forests is difficult due to access limitations in the Tian Shan, remote sensing offers a unique opportunity to increase spatial and temporal coverage of ecological parameters. Sentinel-2 satellites launched in 2015 have been providing images at spatial resolutions of 10 to 20 m; however, difficulties remain as information retrieved from Sentinel pixels result from a mixture of objects that affect reflectance signals. We used submeter multispectral UAV images to assess the sensitivity of Sentinel-2 normalized difference vegetation index (NDVI) to subpixel vegetation. Results showed that Sentinel-2 data overestimates NDVI in regions with open terrain and grass, and underestimates NDVI in areas with trees. By implementing a bias correction method, the accuracy of the Sentinel-2 derived NDVI increased; R^2 values increased from 0.59 to 0.88 (p value < 0.001). We also showed that drought index derived from Sentinel-2 vegetation condition index (VCI) is well correlated with the ground-based standard precipitation index (SPI). Using this bias correction method, on average the correlation increased by 3% between VCI and SPI. © *The Authors. Published by SPIE under a Creative Commons Attribution 4.0 International License. Distribution or reproduction of this work in whole or in part requires full attribution of the original publication, including its DOI.* [DOI: 10.1117/1.JRS.17.022204]

1 Introduction

Kyrgyzstan is a mountainous country with rich biodiversity. Although it occupies only 0.13% of the Earth land surface, Kyrgyzstan has about 2% of the world's floral and 3% of its faunal diversity.[1] Also many wild fruits and flowers originate from this region with a wide range of genetic diversity related to widely cultivated plants like tulips[2,3] and apples.[4] Moreover, Kyrgyzstan is a poor country with more than 60% of its population residing in rural areas.[5] Wild walnut-fruit forests in the south play an important role in the rural economy, which are effectively the main sources of income for many families in the villages, surpassing animal husbandry. Walnut (*Juglans regia*) is the main crop, which is being harvested on annual basis by local residents; however, wild apples also contribute to the incomes of rural families. Forest products contribute from 22% to 61% of local incomes with walnut collection being the most significant source followed by wild apples.[6,7]

The most numerous wild apple species is *Malus sieversii*; red apples (*Malus niedzwetzkyana*) are far less abundant (<10% of apple trees). Both *Malus* species are included in the Red Data Book of Kyrgyzstan.[1] *Malus niedzwetzkyana* is rated as "vulnerable" in national Red Data Book and "endangered" by the IUCN Global Red List; *Malus sieversii* is categorized as "least concern" and "vulnerable," respectively, on the two lists. *Malus sieversii* is considered an ancestor of *Malus orientalis* and *Malus domestica*, a domestic variety of apple trees,[4] which makes it a valuable genetic resource for new varieties.

---

*Address all correspondence to Erkin Isaev, erkin.isaev@ucentralasia.org

Livestock that browse freely in these forests destroy young trees and damage stems and branches of adult trees.[8–10] Overgrazing and selective cutting for firewood contributes to suppression of natural regeneration and loss of genetic diversity.[11,12] In addition to these anthropogenic influences, climate change is increasing drought occurrence frequency and thus changing natural habitats.[13–16] Kyrgyzstan is the third most vulnerable country in Eastern Europe and Central Asia to climate change, mainly owing to its climate-sensitive agricultural systems and a lack of an adaptive capacity.[17]

If no measures are taken, the sparse populations of wild apples can be severely damaged and further decreased. Thus accurate spatial and temporal monitoring of trees is important to protect natural ecosystems. In addition, accurate estimates of the extent of degraded forests and forest clearing are key components of international climate change initiatives, such as reducing emissions from altered and transformed forests in developing countries (REDD+) within the context of the UN framework convention on climate change.[18] As selective logging and collection of nontimber forest products are widespread, it is imperative to develop a national or subnational system that accurately monitors forest canopy openings, intensity of use, and contributes to improved forest management to recover forest biomass (carbon stocks) and natural regeneration.[19]

Remotely sensed data provide a great potential for analyzing Earth surface dynamics at various spatiotemporal scales, particularly in areas that are challenging to access.[20] Knowledge of spatial variability among and within forest parcels is a key factor for the users of walnut fruit forests to estimate yield and quality.[21] In this context, remote sensing (RS) has already shown its potential and effectiveness in spatiotemporal vegetation monitoring.[19,22–24] Additionally, many satellite platforms (e.g., Landsat, MODIS, Aster, SPOT, Sentinel-1, and Sentinel-2) are now providing free datasets, thus promoting satellite imagery for many agricultural applications,[14,22,23,25–27] including those with multisensor data fusion approachs.[28] For example, remotely sensed images from Sentinel-2 used in our research offer decametric resolution in terms of space and time, with a ground sample distance of up to 10 m and a revisit time of 6 days. Misregistration of Sentinel-2 imageries was addressed in the processing baseline (version 02.04)[21] and deployed by the European Space Agency on June 15, 2016.[29]

However, when considering vegetation over complex terrain, such as mountainous Kyrgyzstan with 94% of the land occurring above 1000 m a.s.l.,[30] RS becomes more challenging. Indeed, steep and complex orography leading to varying lighting conditions may deeply affect the computation of the overall spectral indices leading to a biased vegetation status assessment. Therefore, approaches and algorithms using unmanned aerial vehicles (UAV) have been developed for satellite-based multispectral vegetation pixel calibration over mountainous regions. Low-altitude platforms, such as UAV and airborne sensors, provide imagery with high spatial resolution (up to a few cm) and flexible flight scheduling[31] facilitating vegetation monitoring at high resolution in complex terrain.

Recent studies applied UAVs in assessing forest condition,[19,32–34] precision agriculture,[21,23,24,35] and mapping, modeling, and monitoring landslides.[36–43] Several approaches have been employed to calibrate satellite imagery with UAV multispectral data and field radiometric measurements. These focus on improving the satellite multispectral imagery to facilitate use in precise monitoring of large agricultural areas by calibrating spectral bands[44,45] or calibrating vegetation indices.[35,46] Some studies have improved satellite reconnaissance data on physical characteristics of vegetation (e.g., leaf area index) using UAV data.[47,48] Other studies solve the practical issue of mapping of invasive species with combinations of UAV and Sentinel imagery and application of machine learning approaches.[49] Our understanding of forest vegetation phenology has also improved by calibrating satellite-derived vegetation and imagery index time series with images derived from UAV and spectral reflectance sensors.[50] Another study used RGB (red, green, and blue) images derived from consumer grade UAVs to more precisely identify riparian forests from Sentinel image time series.[51] Other recent investigations focused on the alignment among different spectral bands of Landsat, Sentinel, PlanetScope, and UAV (MicaSense) images on various surface categories in urban areas, providing an exhaustive comparison of spectral band matching,[52] and atmospheric correction of satellite images with UAV-sensed normalized difference vegetation index (NDVI).[53] All these studies show the viability and practical applicability of employing satellite imagery correction with UAV imagery because

UAV imagery is more accurate due to its proximity to the observation point and there is no need for atmospheric correction.

The scope of this work is to compare Sentinel-2 and UAV imagery from Western Tian Shan for monitoring applications in walnut fruit forests with a practical aim to improve forest management and species conservation. In this research, a detailed analysis and comparison of products provided by a decametric resolution satellite and a low-altitude centimetric resolution UAV platform is presented. We developed an RS-based approach to calibrate Sentinel-2 data at a study site in Western Tian Shan using UAV data. The effectiveness of Sentinel-2 data bias correction was evaluated by considering the well-known relation between the NDVI, vegetation condition index (VCI), and standard precipitation index (SPI).

2 Materials and Methods

2.1 *Study Site*

The study was conducted in the western Tian Shan (Fig. 1) on slopes of the Fergana and Chatkal ranges. More specifically, the investigated areas are: Sary-Chelek biosphere reserve, Padysha-Ata nature reserve, and Kara-Alma forestry unit. These areas are recognized as key biodiversity areas (KBA) by the Critical Ecosystem Partnership Fund (Table 1).

The western slopes of Fergana range and southern slopes of Chatkal range in the south of Kyrgyzstan are covered with unique fruit and nut forests, occupying elevations ranging from about 1000 to 2500 m a.s.l. These semiwild forests are dominated by walnut (*Juglans regia*) trees with patches of wild apple (*Malus sieversii* and *M. niedzwetzkyana*) and wild pear (*Pyrus korshinskyi*), which are globally threatened. *Abies semenovii* and *Picea schrenkiana* can be found in mixed forests on hillslopes. Other scattered tree species also grow in this forest, but
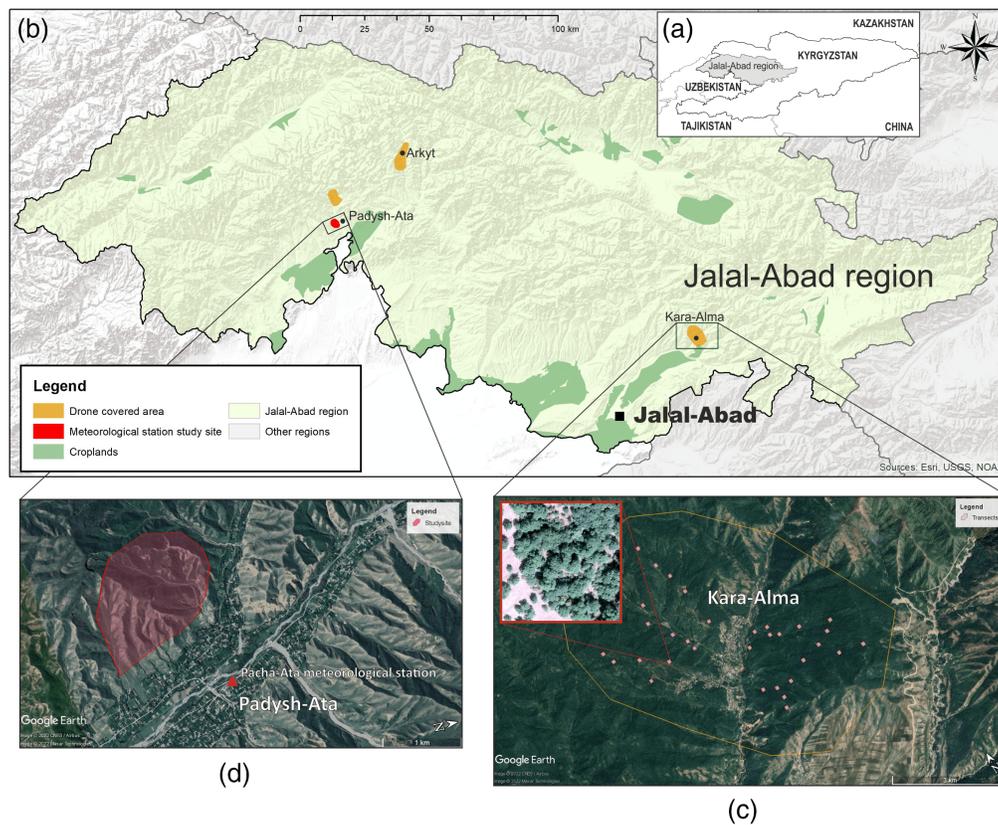
Fig. 1 Study site locations: (a) within Kyrgyzstan; (b) Jalal-Abad region with croplands and area covered by UAV; (c) UAV image example from Padysha-Ata nature reserve; and (d) Pacha-Ata meteorological station showing the study polygon.

Table 1 West Tian-Shan KBA.

Name	KBA_ID	Coordinates	Area (km^2)	Description
Sary-Chelek	KGZ06	Lon: E71.933132° Lat: N41.868115°	237.96	UNESCO biosphere reserve on south slope of Chatkal range in the south of Kyrgyzstan
Padysh-Ata	KGZ05	Lon: E71.683163 deg Lat: N41.717878 deg	680.55	Padysha-Ata nature reserve on the south slope of Chatkal range
Kara-Alma	KGZ18	Lon: E73.341518 deg Lat: N41.249517 deg	267.6	Kara-Alma forestry unit has the largest population of wild apple trees, on the western slope of Fergana range

they do not develop forest patches and are distributed sporadically within the walnut and apple forests. These scattered species include *Acer turkestanicum, Pyrus turcomanica, Crataegus* spp., *Betula* spp., *Populus* spp., *Fraxinus* spp., *Prunus sogdiana, Lonicera* spp., *Berberis* spp., *Cotoneaster* spp., *Rosa* spp., and among others.

2.2 Datasets

UAV images were acquired using a built-in multispectral camera onboard a DJI Phantom 4 Multispectral. The drone's camera features one RGB sensor and five multispectral sensors red (R), green (G), blue (B), red edge (RE), and near-infrared (NIR). It can provide cm-scale mapping accuracy using high-resolution multispectral images. The drone also has a sunlight sensor on the top to capture lighting intensity, which is used for lighting correction, thus providing more consistent and comparable data collection results.

The flights were conducted in July and August 2021, each covering an area of 105×105 m, at an altitude of 50 m above the take-off point with a 90% front overlap, and an 80% side overlap. This results in $\sim$2.6 cm resolution on the ground and potentially higher resolution at treetops. The plots were selected to cover the greatest vegetation variability in the study region. In total, we conducted 59 drone flights over different 11,025 m^2 plot areas.

Sentinel-2 images (Sentinel-2 MSI: MultiSpectral Instrument, Level-1C) (Table 2) available from the Google Earth Engine platform were used in this analysis. We used all available data from Sentinel-2 scenes with <5% cloud cover acquired between April and September of 2016 to 2021.

Data on annual crop yields for the Jalal-Abad region were obtained from Kyrgyz Statistic Comity.[5] These datasets include information on grains, wheat, barley, corn, rice, sugar-beet, cotton, tobacco, vegetable oils, potatoes, vegetables, melons, fruits and berries, and grapes from 1990 until 2021. These data were used for verification, which is described later.

Meteorological data were obtained from the previous research by Kyrgyzhydromet on droughts in Kyrgyzstan[13] and from decadal agrometeorological bulletins.[54] The data represent monthly precipitation from 1981 to 2021 collected by Kyrgyzhydromet at Pacha-Ata meteorological station.

2.3 Methodological Approach

2.3.1 Automatic photogrammetric adjustments

Photogrammetric adjustments and the development of orthomosaic UAV images were conducted using Agisoft Metashape 1.8.3 Professional Edition.[55] This software uses the coordinates of exposure centers of each image performing aerial triangulation in each cell and reconstructs the photogrammetric blocks.[19] It also conducts automatic lightning adjustments of scenes based on the information from the UAV lightning sensor. These adjustments ensure data consistency among flights. Finally, we obtained 59 multispectral orthomosaics, which were resampled to a 2-cm spatial resolution and 100×100 m tile size. Specific information regarding the camera and image overlays of the UAV image processing is presented in Table 3.

Table 2 Characteristics of the RS UAV and Sentinel-2: MSI, multispectral instrument, level-1C datasets.

|	Sentinel-2 A/B		DJI Phantom 4 multispectral		
Name	Pixel size (m)	Wavelength (nm)	Wavelength (nm)	Pixel size (cm)	Description
B1	60	443.9 (S2A)/442.3 (S2B)	—	—	Aerosols
B2	10	496.6 (S2A)/492.1 (S2B)	450 ± 16	2	Blue
B3	10	560 (S2A)/559 (S2B)	560 ± 16	2	Green
B4	10	664.5 (S2A)/665 (S2B)	650 ± 16	2	Red
B5	20	703.9 (S2A)/703.8 (S2B)	—	—	Red edge 1
B6	20	740.2 (S2A)/739.1 (S2B)	730 ± 16	2	Red edge 2
B7	20	782.5 (S2A)/779.7 (S2B)	—	—	Red edge 3
B8	10	835.1 (S2A)/833 (S2B)	840 ± 26	2 cm	NIR
B8A	20	864.8 (S2A)/864 (S2B)	—	—	Red edge 4
B9	60	945 (S2A)/943.2 (S2B)	—	—	Water vapor
B10	60	1373.5 (S2A)/1376.9 (S2B)	—	—	Cirrus
B11	20	1613.7 (S2A)/1610.4 (S2B)	—	—	SWIR 1
B12	20	2202.4 (S2A)/2185.7 (S2B)	—	—	SWIR 2
QA10	10	—	—	—	Always empty
QA20	20	—	—	—	Always empty
QA60	60	—	—	—	Cloud mask

Table 3 Parameters used in the Agisoft Metashape software for image orthomosaic generation and georeferencing the UAV image of the study site.

Attribute	Value
Number of scenes per tile	∼410
Number of tiles	59
Flight altitude	50 m
Image resolution	0.02 m pixel^{-1}
Coverage area (tile size)	100 × 100 m
Spectral channels	Red, green, blue, red edge, and NIR

NDVI was calculated in Agisoft Metashape with a raster calculator as follows:

$$\text{NDVI} = \frac{(\text{NIR} - \text{Red})}{(\text{NIR} + \text{Red})}, \tag{1}$$

where NIR is the near-infrared band and Red is the red band. We used only NDVI images in the analysis. The UAV image composite [Fig. 2(a)] allowed us to identify individual trees, whereas
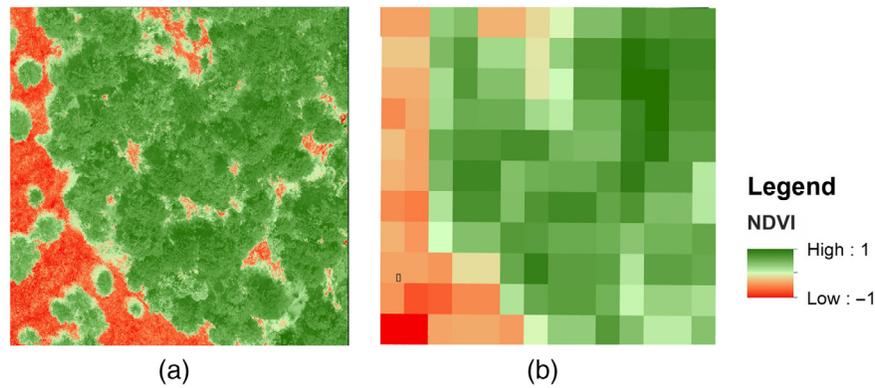
Fig. 2 One tile of the remotely sensed images of the study site (August 2021): (a) UAV NDVI image (0.02 m spatial resolution) and (b) Sentinel-2 NDVI image (10 m spatial resolution).

the corresponding NDVI image sections derived from Sentinel-2 [Fig. 2(b)] imagery showed much less detail.

2.3.2 *Data processing*

In this section, specific methods for data processing developed to compare and investigate the imagery derived from the two platforms with different spatial resolutions are presented and discussed in detail.

We calculated NDVI with Sentinel-2 data according to Eq. (1) in Google Earth Engine for the dates closest to the UAV flights with <10% of the scene covered with clouds. As a result, 59 Sentinel-2 NDVI tiles with areas of about 100×100 m were obtained [Fig. 3(a)], which were overlapped with UAV NDVI tiles. However, because the spatial resolution of Sentinel-2 images is 10 m and that of UAV images is 0.02 m, the pixels did not always overlap—i.e., not all UAV pixels fell entirely into Sentinel-2 pixels, and sometimes Sentitel-2 tiles were larger than UAV tiles because pixel size caused a fragmentation problem (Fig. 3). Thus we omitted these fragmented pixels from further analysis. For each, tile we generated a polygon grid with each cell exactly representing pixels of Sentinel-2 images overlayed on the UAV images [Figs. 3(a) and 3(b)]. For each unfragmented cell, the mean NDVI value of each UAV image was calculated.

2.3.3 *Bias correction*

To assess the spatial patterns on bias distribution, we calculated NDVI difference between Sentinel and UAV mean values for each Sentinel pixel as

$$\mathrm{NDVI}_{\mathrm{diff}(x,y)} = \mathrm{NDVI}_{\mathrm{Sent}(x,y)} - \mathrm{NDVI}_{\mathrm{UAV}(x,y)}, \tag{2}$$
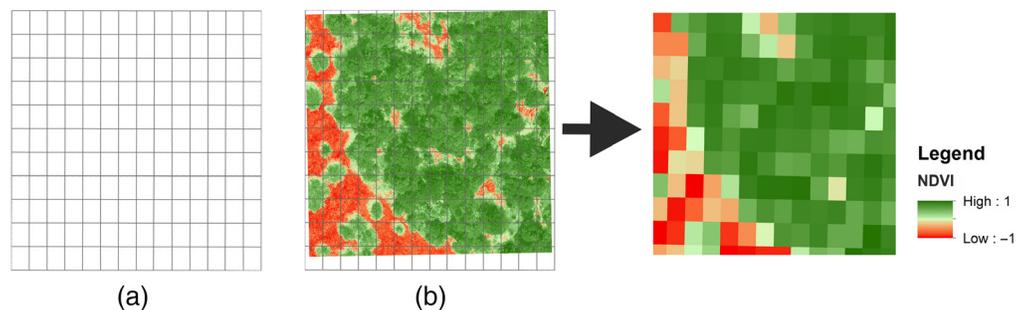
Fig. 3 (a) Ordered grid of pixels from Sentinel-2 and (b) polygon grid example highlighted with black.

where (x, y) are the pixel coordinates in Sentinel-2 and the overlayed UAV NDVI, $\text{NDVI}_{\text{diff}}$ is the difference in NDVI values between Sentinel-2 and UAV images, $\text{NDVI}_{\text{Sent}}$ are NDVI values calculated from Sentinel-2 images, and NDVI_{UAV} are NDVI values calculated from UAV images. To assess potential errors, mean error (ME)

$$\text{ME} = \frac{1}{n}\sum_{i=1}^{n}(\text{NDVI}_{\text{Sent}} - \text{NDVI}_{\text{UAV}}) \tag{3}$$

and the square root-mean-squared error (RMSE) were calculated:

$$\text{RMSE} = \sqrt[2]{\frac{1}{n}\sum_{i=1}^{n}(\text{NDVI}_{\text{Sent}} - \text{NDVI}_{\text{UAV}})^2}. \tag{4}$$

To assess systematic patterns in errors for overestimation and underestimation of NDVI, we selected all the pixels with absolute values of $\text{NDVI}_{\text{diff}}$ greater then RMSE (i.e., pixels with significant error) and divided them into pixels with positive ($\text{NDVI}_{\text{diff}} > 0$) and negative ($\text{NDVI}_{\text{diff}} < 0$) errors, comprising overestimation and underestimation of NDVI by Sentinel-2. For all pixels with significant negative $\text{NDVI}_{\text{diff}}$, we have calculated spatial maximum and minimum NDVI values (NDVI_{max} and NDVI_{min}), comprising the upper and lower NDVI envelopes of underestimated values [see Eqs. (5) and (6)]. Likewise, for all the pixels with significant positive $\text{NDVI}_{\text{diff}}$, we calculated spatial maximum and minimum NDVI values (NDVI_{max} and NDVI_{min}), comprising the upper and lower NDVI envelopes of overestimated values [see Eqs. (7) and (8)]:

$$\text{UNE} = \text{NDVI}_{\text{max}(x,y)} \quad \forall\,(x,y) \in (|\text{NDVI}_{\text{diff}(x,y)}| > \text{RMSE}) \cap (\text{NDVI}_{\text{diff}(x,y)} < 0), \tag{5}$$

$$\text{LNE} = \text{NDVI}_{\text{min}(x,y)} \quad \forall\,(x,y) \in (|\text{NDVI}_{\text{diff}(x,y)}| > \text{RMSE}) \cap (\text{NDVI}_{\text{diff}(x,y)} < 0), \tag{6}$$

$$\text{UPE} = \text{NDVI}_{\text{max}(x,y)} \quad \forall\,(x,y) \in (|\text{NDVI}_{\text{diff}(x,y)}| > \text{RMSE}) \cap (\text{NDVI}_{\text{diff}(x,y)} > 0), \tag{7}$$

$$\text{LPE} = \text{NDVI}_{\text{min}(x,y)} \quad \forall\,(x,y) \in (|\text{NDVI}_{\text{diff}(x,y)}| > \text{RMSE}) \cap (\text{NDVI}_{\text{diff}(x,y)} > 0), \tag{8}$$

where (x, y) are the values at pixel coordinates x, y, UNE represents the upper negative envelope, LNE is the lower negative envelope, UPE is the upper positive envelope, and LPE is the lower positive envelope.

As previously noted, we developed different bias correction rates for values of NDVI $\in$ (LNE, UNE) and NDVI $\in$ (LPE, UPE). All the NDVI values outside of these ranges are assumed not to require bias correction, as the error is less than RMSE. We used RMSE and ME for bias correction to compare which of these metrics perform better. The following equation represents this approach with RMSE; the same was conducted with ME:

$$\text{NDVI}_{\text{Sent}}^{\text{corr}} = \begin{cases} \text{NDVI}_{\text{Sent}} + \text{RMSE}, & \text{NDVI}_{\text{Sent}} \in (\text{LNE, UNE}), \\ \text{NDVI}_{\text{Sent}} - \text{RMSE}, & \text{NDVI}_{\text{Sent}} \in (\text{LPE, UPE}), \\ \text{NDVI}_{\text{Sent}}, & \text{NDVI}_{\text{Sent}} \neg \in (\text{LPE, UPE}) \cup (\text{LNE, UNE}), \end{cases} \tag{9}$$

where $\text{NDVI}_{\text{Sent}}^{\text{corr}}$ is the bias-corrected Sentintel-2 NDVI.

2.4 Verification of Bias Correction

2.4.1 Verification of bias correction with VCI and SPI

To verify the accuracy gained from bias correction, we calculated VCI using a method proposed by Kogan[56] for NDVI values with and without correction:

$$\text{VCI}_{(x,y,t)} = \frac{\text{NDVI}_{(x,y,t)} - \text{NDVI}_{\text{min}(x,y,n)}}{\text{NDVI}_{\text{max}(x,y,n)} - \text{NDVI}_{\text{min}(x,y,n)}} \times 100\%, \tag{10}$$

where (x, y, t) are the values at pixel coordinates x, y at a certain time t (month), (x, y, n) are the vector values at pixel coordinates x, y for the entire period of observation n, $\text{VCI}_{(x,y,t)}$ are the vegetation condition index values for specified pixels at times (month), and $\text{NDVI}_{\min(x,y)}$ and $\text{NDVI}_{\max(x,y)}$ are the monthly minimum and maximum NDVI values for many years (from April to September from 2016 to 2021) for each pixel.

The area near Pacha-Ata meteorological station [Fig. 1(d)] was selected to assess and verify the bias correction methods for Sentinel-2 because it is representative of the ecosystem and proximate to UAV plots and the meteorological station. Monthly SPI values were calculated using monthly precipitation data from Pacha-Ata meteorological station for the period 1981 to 2021. We used SPI drought index, which was verified in a Kyrgyzhydromet study[13] as the best drought index for Kyrgyzstan.

In 2009, the World Meteorological Organization (WMO) recommended using SPI for drought monitoring, which has been adopted in research or operational practice by more than 70 countries.[57] "SPI depth" denotes the precipitation sum for the number of months used in the calculation. WMO recommends using the following SPI depth classification for detecting different drought types: 1 or 2 months for meteorological drought, 3 to 6 months for agricultural drought, 6 to 12 months, or more for monitoring hydrological drought.[57]

We calculated NDVI from Sentinel-2 and then conducted NDVI bias correction with two methods (RSME and ME) [Eq. (11)] for vegetation growing season April to September 2016 to 2021. Next, we calculated the spatial mean of corrected NDVI images for each month followed by calculating Pearson's correlation coefficients between corrected NDVI spatial means and SPI with different depths (1 to 12). The delayed response of vegetation to precipitation creates correlation lags in the time series, thus, correlation coefficients were calculated with different monthly shifts of corrected NDVI and VCI versus SPI.[58]

### 2.4.2 *Verification of bias correction with crop yield*

To verify corrected NDVI from Sentinel-2 with ground data, we compared mean annual corrected NDVI on croplands of Jalal-Abad province for the vegetation growing season (April to September of 2016 to 2021) with the crop yield productivity for the province (from the National Statistical Committee of Kyrgyz Republic). We conducted correlation analysis of yield of different crops and SPI for September with different SPI depths to identify which crops are most related to precipitation and drought; these crops were then used to validate the NDVI correction. Only September was selected for the SPI calculation as this month is most representative for yield approximations.[13] However, since only six annual NDVI observations (2016 to 2021) were available, we could not conduct a proper significant correlation analysis, so we applied a qualitative visual assessment of the relation between NDVI and crop yield data.

3 Results

3.1 *Bias Correction*

After our qualitative visual analysis of $\text{NDVI}_{\text{diff}}$ [Eq. (2)] on 59 UAV images, we determined that Sentinel-2 overestimates NDVI in the areas with open terrain and grass (low NDVI values), and underestimates NDVI in the areas with trees (high NDVI values). The error analysis [Eqs. (3) and (4)] resulted in the following: RMSE = 0.1228 and ME = −0.077. The relation between $\text{NDVI}_{\text{Sent}}$ and NDVI_{UAV} is positive [Figs. 4(a) and 4(b)]. The linear regression model yielded an $R^2 = 0.59$ and a p value < 0.001 [Fig. 4(a)] on uncorrected data. The envelope interval estimates were: LNE = 0.6, UNE = 0.8, LPE = 0.5, and UPE = 0.6. After implementation of the bias correction with RMSE and ME for Sentinel-2 using Eq. (9), the accuracy of the Sentinel-2 derived NDVI increased [Fig. 4(b)].

Verification with VCI indicates that using RMSE for bias correction of NDVI provides better results than ME (Table 4). After correction, R^2 increased to 0.88 with p value < 0.001 [Fig. 4(b)]. Thus we describe the bias correction by the following conditional equation:
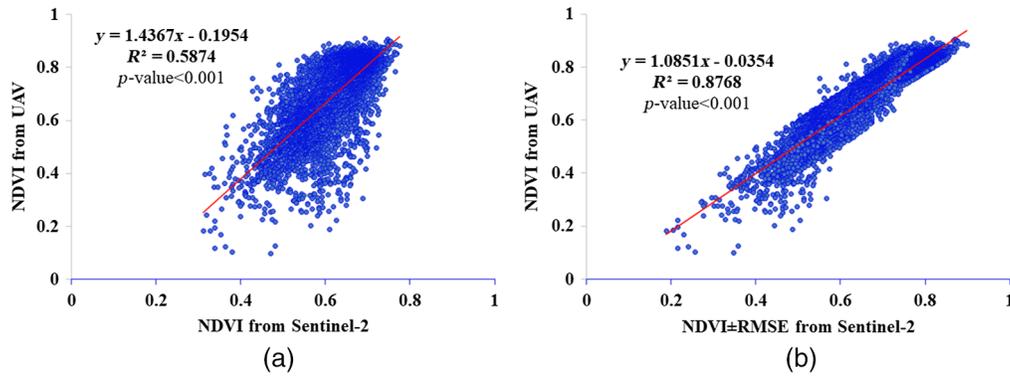
Fig. 4 Relation between NDVI derived from Sentinel-2 and NDVI derived from UAV imagery; number of pixels = 6486: (a) Sentinel-2 without bias correction and (b) Sentinel-2 with bias correction.

Table 4 Correlation coefficients between Sentinel-2 derived corrected and uncorrected NDVI and VCI with 0- and 1-month lag, and SPI indices with depth from 1 to 12 months; bold coefficients are the significant ones with $p < 0.05$.

	SPI1	SPI2	SPI3	SPI4	SPI5	SPI6	SPI7	SPI8	SPI9	SPI10	SPI11	SPI12
VCI	0.13	**0.40**	0.31	0.30	0.26	0.28	0.25	0.33	**0.37**	**0.36**	**0.36**	0.34
VCI$_{\text{Corr-RMSE}}$	0.13	**0.41**	0.31	0.31	0.27	0.31	0.27	**0.35**	**0.39**	**0.37**	**0.37**	**0.35**
VCI$_{\text{Corr-ME}}$	0.13	**0.40**	0.31	0.30	0.26	0.28	0.25	0.33	**0.37**	**0.36**	**0.36**	0.34
VCI$_{+1\text{month}}$	**0.41**	**0.36**	0.28	0.21	0.25	0.22	0.28	**0.35**	**0.37**	**0.38**	**0.36**	**0.39**
VCI$_{\text{Corr-RMSE+1month}}$	**0.42**	**0.36**	0.29	0.22	0.28	0.24	0.29	**0.37**	**0.37**	**0.40**	**0.37**	**0.42**
VCI$_{\text{Corr-ME+1month}}$	**0.41**	**0.36**	0.28	0.21	0.25	0.22	0.28	**0.35**	**0.37**	**0.38**	**0.36**	**0.39**
NDVI	0.05	0.09	0.12	0.11	0.11	0.07	0.10	0.08	0.10	0.17	0.13	0.13
NDVI$_{\text{Corr-RMSE}}$	0.02	0.11	0.14	0.13	0.12	0.10	0.13	0.11	0.13	0.19	0.16	0.15
NDVI$_{\text{Corr-ME}}$	0.05	0.09	0.12	0.11	0.11	0.07	0.10	0.08	0.10	0.17	0.13	0.13
NDVI$_{+1\text{month}}$	0.22	0.29	0.17	0.17	0.14	0.16	0.17	0.22	0.25	0.25	0.21	0.19
NDVI$_{\text{Corr-RMSE+1month}}$	0.20	0.27	0.16	0.16	0.14	0.17	0.18	0.22	0.25	0.25	0.20	0.21
NDVI$_{\text{Corr-ME+1month}}$	0.22	0.29	0.17	0.17	0.14	0.16	0.17	0.22	0.25	0.25	0.21	0.19

$$\text{VI}_{\text{Sent}}^{\text{corr}} = \begin{cases} \text{NDVI}_{\text{Sent}} + 0.1228, & \text{NDVI}_{\text{Sent}} \in [0.6, 0.8], \\ \text{NDVI}_{\text{Sent}} - 0.1228, & \text{NDVI}_{\text{Sent}} \in [0.5, 0.6), \\ \text{NDVI}_{\text{Sent}}, & \text{NDVI}_{\text{Sent}} \neg \in [0.5, 0.6) \cup [0.6, 0.8] \end{cases}. \quad (11)$$

3.2 Verification of Bias Correction with VCI

To verify the bias-corrected NDVI with VCI, we calculated correlations between SPI indices and NDVI with VCI for the area near Pacha-Ata meteorological station [Fig. 1(d)] and the climatic data from that station indicates that correlation increases between VCI and SPI when corrected NDVI Sentinel-2 data are used (Table 4). In general, correction of NDVI with RMSE indicates in better results than with ME (Table 4). Therefore, RMSE correction was used for the final bias correction [Eq. (11)].

When calculated vegetation indices are shifted by one month the correlation relationship increased because precipitation affects vegetation with approximately a 2- to 3-week lag period. The highest correlation was obtained between VCI corrected with RMSE and a 1-month lag with

SPI1 and SPI12 ($r = 0.42$, $p < 0.05$), which shows the rate of precipitation in one month relative to the multiyear norm (Table 4). The correlation coefficients between vegetation indices with 2- and 3-month lags, and SPI were less than those with a 1-month lag, so they are not reported in the results.

3.3 *Verification of Bias Correction with Crop Yields*

Using yield productivity data for different crops in Jalal-Abad province together with correlating with SPI indices for September, we identified that wheat and barley are the crops most related to precipitation and drought (Table 5). Thus these crops were used for verification of NDVI correction.

The highest correlation coefficients between yield and SPI are between barley/wheat and SPI6. The significant correlation is between barley and SPI6 with $r = 0.35$, $p < 0.05$. A qualitative visual assessment of yield related to bias corrected NDVI was only possible due to insufficient sample size (Fig. 5).

The same tendency of the bias corrected NDVI and yield productivity is evident (Fig. 5). The corrected annual NDVI curve is smoother than the uncorrected one and is in closer agreement with the annual yield curve of barley and wheat (Fig. 5). The maximum yields for wheat and barley in 2018 were 2.7 metric tons per hectare and 2.1 metric tons per hectare, respectively, and NDVI with bias correction was 0.38. The minimum yields for wheat and barley in 2021 were 2.2 metric tons per hectare and 1.7 metric tons per hectare, respectively, and NDVI with bias correction was 0.31.

4 Discussion

Although most of forest, cropland, and pasture datasets are based on RS observations, the analysis of vegetation succession still relies largely on fieldwork in a space-for-time framework without the benefit of important historical remotely sensed information, with some exceptions.[26] Nonetheless, challenges remain in the search of an optimal and reliable relationship between

Table 5 Correlation coefficients between yield productivity (metric tons per hectare from 1991 to 2021) and SPI indices; SPI with depth from 1 to 12 months; Bold coefficients are significant ($p < 0.05$).

|	SPI1	SPI2	SPI3	SPI4	SPI5	SPI6	SPI7	SPI8	SPI9	SPI10	SPI11	SPI12
Grains	0.15	0.09	−0.13	−0.09	−0.08	−0.02	−0.04	−0.09	−0.08	−0.21	−0.21	−0.21
Wheat	0.25	0.32	0.20	0.14	0.16	0.26	0.14	0.09	0.05	0.22	0.22	0.22
Barley	0.26	0.33	0.11	0.24	0.29	**0.35**	0.27	0.22	0.19	-0.01	-0.02	-0.01
Corn	0.15	0.14	0.07	0.05	0.04	0.13	0.11	0.07	0.08	-0.08	-0.09	-0.09
Rice	0.19	0.16	−0.13	−0.09	−0.12	−0.06	−0.09	−0.14	−0.10	−0.15	−0.16	−0.16
Cotton	0.11	0.13	−0.11	−0.02	−0.04	0.03	0.02	−0.03	−0.02	−0.08	−0.08	−0.08
Tobacco	0.14	0.21	0.30	0.02	0.04	0.00	0.02	-0.02	-0.04	0.10	0.10	0.10
Vegetable oils	0.18	0.18	0.05	−0.01	−0.05	−0.01	−0.02	−0.07	−0.03	−0.06	−0.06	−0.06
Potatoes	0.22	0.16	−0.01	−0.05	−0.05	−0.01	−0.01	−0.03	0.00	−0.12	−0.12	−0.12
Vegetables	0.15	0.16	−0.11	−0.03	−0.03	0.01	0.00	−0.05	−0.01	−0.16	−0.16	−0.16
Melons	0.13	0.13	−0.05	−0.05	−0.05	−0.03	−0.03	−0.09	−0.04	−0.17	−0.17	−0.17
Fruits and berries	0.11	0.00	−0.10	−0.15	−0.13	−0.11	−0.12	−0.17	−0.13	−0.16	−0.16	−0.16
Grapes	−0.21	−0.12	−0.04	−0.09	−0.12	−0.09	−0.14	−0.14	−0.18	0.15	0.15	0.16
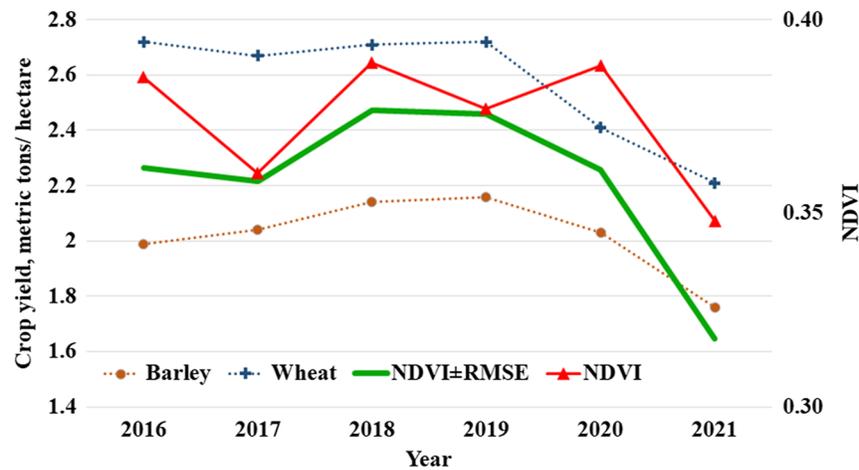
Fig. 5 Crop yield and NDVI time series for Jalal-Abad region (spatially averaged).

remotely detected changes in vegetation indices (e.g., NDVI and VCI) and actual vegetation changes on the ground.

We found that decametric resolution satellite imagery had limitations in directly providing reliable information on the status of walnut-fruit forests in the Western Tian Shan. This effect was confirmed by the improved relation found between the corrected satellite derived NDVI and the NDVI derived from UAV surveys in contrast to the original relation [Fig. 4(a)]. Sentinel-2 data overestimates NDVI in areas with open terrain and grass, and underestimates NDVI in areas with trees. However, the accuracy of Sentinel-2 derived NDVI increased by implementing a bias correction based on RMSE for different NDVI intervals: $0.5 < NDVI < 0.6$ with negative RMSE and $0.6 < NDVI < 0.8$ with positive RMSE [Fig. 4(b)], and R^2 increased to 0.88 with a p value < 0.001 [Fig. 4(b)]. However, using UAV together with field spectroradiometry can yield a greater spectral band coherence of RSME $< 1\%$.[44] High LAI estimation accuracy (R^2 values up to 0.88) was also obtained in other studies.[47]

In addition, we found that drought index derived from RS, data are well correlated with ground-based SPI drought index. Using our proposed bias correction method, the correlation between VCI and SPI increased by 3% on average (Table 4). Moreover, shifting VCI by 1-month ahead of precipitation data yielded the highest correlation with SPI indices. This shift in vegetation response relative to precipitation has also been observed by other studies.[58–61]

The highest correlation relations between crop yield and SPI drought indices were obtained for barley and wheat. A significant correlation was found between barley yield and SPI6 ($r = 0.35$). Barley and wheat are mostly cultivated on unirrigated lands; thus they tend to be more correlated with drought index SPI. According to WMO recommendations, SPI6 determines agriculture drought (soil drought) which is indicative of yield response to drought. Other crops, such as corn, rice, cotton, tobacco, vegetables, potatoes, vegetable oil crops, melons, fruits, and berries, are grown in flatter, irrigated lands and thus their yields are less affected by meteorological and soil droughts. Bias corrected NDVI replicated barley and wheat yield productivity well (Fig. 5).

We assumed that the extremely high spatial resolution due to the near ground surface UAV surveys provided a "ground truth" quality layer with respect to Sentinel-2 imagery. Nonetheless, true field data collection coupled with hyperspectral imagery would still be required to further investigate the effects of complex and steep topography on Sentinel derived NDVI values. Furthermore, the spectral bands of DJI Phantom 4 Multispectral and Sentinel-2 a/b are not identical (Table 2), which contributes some uncertainty. However, our findings are a clear step forward from previous studies that used Phantom quadcopters adapted and equipped with third-party cameras,[46] notwithstanding the results of this research.

Despite the lack of consideration of certain factors discussed herein, we are confident that our work is an advance in understanding how the combination of UAV and satellite RS methods can improve the monitoring of droughts, pastures, croplands, and walnut fruit forest conditions.

Because other investigations obtained similar results in terms of Sentinel-2 sensitivity to vegetation cover,[23,24] we are confident that our analysis is relevant for other mountains regions and that the bias correction method can be used to correct the Sentinel-2 images to obtain improved results in other similar contexts. Our findings can thus be used to improve management of forest resources and contribute to conservation of rare and threatened tree species.

5 Conclusions

In this study, Sentinel-2 satellite images were compared with imagery from a UAV equipped with a multispectral camera to evaluate both techniques based on NDVI and VCI indices.

The statistical comparison between Sentinel-2 and UAV imagery shows that the followings.

- The trend of the average NDVI is almost identical for both RS techniques.
- There is a strong correlation of the NDVI indices between the two techniques.
- The implementation of a bias correction method significantly increases NDVI and VCI indices derived from Sentinel-2.

Both UAV and Sentinel-2 platforms provide important information for the vegetation cover of mountains, and they are important tools for the monitoring and managing walnut-fruit forests, pastures, and croplands in Kyrgyzstan and similar mountainous regions. The choice of the most appropriate technology (UAV or satellite) depends on the use and the aim of the data collection, as they have different spatial and temporal characteristics, costs, and requirements. But using proposed bias correction method, we can significantly increase accuracy of the Sentinel-2 data.

Acknowledgments

Code, Data, and Materials Availability

The data that support the findings of this study are available from the corresponding author, upon reasonable request.

References

1. SAEPF, IBP-NAS-KR, and Aleine, *Kyrgyz Republic Red Data Book*, 2nd ed., A. Davletkeldiev et al., eds., FAO NFPF, Bishkek (2006).
2. Z. P. Botschantzeva and H. Q. Varekamp, *Tulips: Taxonomy, Morphology, Cytology, Phytogeography and Physiology*, Balkema (1982).
3. B. J. M. Zonneveld, "The systematic value of nuclear genome size for 'all' species of *Tulipa L. (Liliaceae)*," *Plant Syst. Evol.* **281**(1–4), 217–245 (2009).
4. A. Cornille et al., "The domestication and evolutionary ecology of apples," *Trends Genet.* **30**(2), 57–65 (2014).
5. NatStatCom, *Kyrgyzstan. Brief Statistical Handbook*, A. Sultanov et al., eds., Bishkek (2018).
6. K. Dzhakypbekova et al., "The contribution of the underutilised species in the walnut-fruit forests to the local livelihoods in Kyrgyzstan," in *Tropentag, Ghent* (2018).
7. J. Shigaeva et al., Profitability of forest products of walnut-fruit forest of Kyrgyzstan vs agricultural production, case study from Kyzyl Unkur villages, World Mountain Forum, Bishkek (2018).
8. A. Orozumbekov, E. Cantarello, and A. C. Newton, "Status, distribution and use of threatened tree species in the walnut-fruit forests of Kyrgyzstan," *Forest Trees Livelihoods* **24**(1), 1–17 (2014).

9. E. Cantarello et al., "Human impacts on forest biodiversity in protected walnut-fruit forests in Kyrgyzstan," *J. Sustain. Forest* **33**(5), 454–481 (2014).

10. University of Central Asia, "Preserving Wild Apple Species in Western Tian Shan," Web news, 2022, https://ucentralasia.org/news/2022/march/preserving-wild-apple-species-in-western-tian-shan (accessed 1 July 2022).

11. R. Beer et al., "Vegetation history of the walnut forests in Kyrgyzstan (Central Asia): natural or anthropogenic origin?" *Quat. Sci. Rev.* **27**(5–6), 621–632 (2008).

12. P. Borchardt, M. Schmidt, and U. Schickhoff, "Vegetation patterns in Kyrgyzstan's walnut-fruit forests under the impact of changing forest use in post-soviet transformation," *Erde* **141**(3), 255–275 (2010).

13. E. Isaev and S. Omurzakova, "On the possibility of drought detection and modeling in Kyrgyzstan (in Russian)," *Bull. Kyrg. Russ. Slav. Univ.* **11**, 172–176 (2019).

14. S. Park et al., "Assessing climate change impact on cropland suitability in Kyrgyzstan: where are potential high-quality cropland and the way to the future," *Agronomy* **11**(8), 1490 (2021).

15. Z. Kretova, "Assessment of climate change in the Kyrgyz Republic under the IFAD project 'Livestock Development and Market-2'" (2020).

16. "Climate change adaptation in Europe and central Asia: adapting to a changing climate for resilient development," 2018, https://www.adaptation-undp.org/sites/default/files/resources/climate_change_adaptation_in_europe_and_central_asia.pdf (accessed 6 April 2022).

17. K. Erkin Isaev et al., "Reconstruction of hydrometeorological data using dendrochronology and machine learning approaches to bias-correct climate models in northern Tien Shan, Kyrgyzstan," *Water* **14**(15), 2297 (2022).

18. "REDD+ | UNFCCC," https://unfccc.int/topics/land-use/workstreams/reddplus (accessed 1 July 2022).

19. G. Vicente et al., "Assessment of selective logging impacts using UAV, Landsat, and Sentinel data in the Brazilian Amazon rainforest," *Proc. SPIE* **17**(1), 014526 (2022).

20. R. Walcker et al., "Contribution of meandering rivers to natural carbon fluxes: evidence from the Ucayali River, Peruvian Amazonia," *Sci. Total Environ.* **776**, 146056 (2021).

21. A. Khaliq et al., "Comparison of satellite and UAV-based multispectral imagery for vineyard variability assessment," *Remote Sens.* **11**(4), 436 (2019).

22. I. Botvich, A. Shevyrnogov, and D. Emelyanov, "Crop yield map development based on satellite and UAV data," *E3S Web Conf.* **333**, 01001 (2021).

23. N. Bollas, E. Kokinou, and V. Polychronos, "Comparison of sentinel-2 and UAV multispectral data for use in precision agriculture: an application from northern Greece," *Drones* **5**(2), 35 (2021).

24. A. Mancini, E. Frontoni, and P. Zingaretti, "Satellite and UAV data for precision agriculture applications," in *Int. Conf. Unmanned Aircr. Syst. ICUAS 2019*, Institute of Electrical and Electronics Engineers Inc., pp. 491–497 (2019).

25. M. Bobrowski et al., "Application of thermal and phenological land surface parameters for improving ecological niche models of Betula Utilis in the Himalayan region," *Remote Sens.* **10**(6), 814 (2018).

26. A. Bayle et al., "Sensitivity of Landsat NDVI to subpixel vegetation and topographic components in glacier forefields: assessment from high-resolution multispectral UAV imagery," *Proc. SPIE* **15**(4), 044508 (2021).

27. M. Der Yang, S. C. Chen, and H. P. Tsai, "A long-term vegetation recovery estimation for Mt. Jou-Jou using multi-date SPOT 1, 2, and 4 images," *Remote Sens.* **9**(9), 893 (2017).

28. K. A. Semmens et al., "Monitoring daily evapotranspiration over two California vineyards using Landsat 8 in a multi-sensor data fusion approach," *Remote Sens. Environ.* **185**, 155–170 (2016).

29. "New processing baseline (02.04) for Sentinel-2A products – Sentinel Online."

30. E. Isaev et al., "Impact of climate change and air pollution forecasting using machine learning techniques in Bishkek," *Aerosol Air Qual. Res.* **22**(3), 210336 (2022).

31. S. Jay et al., "Exploiting the centimeter resolution of UAV multispectral imagery to improve remote-sensing estimates of canopy structure and biochemistry in sugar beet crops," *Remote Sens. Environ.* **231**, 110898 (2019).

32. A. Ozdarici-Ok et al., "Automated extraction and validation of Stone Pine (*Pinus pinea* L.) trees from UAV-based digital surface models," http://www.tandfonline.com/action/journalInformation?show=aimsScope&journalCode=tgsi20#.VsXpLiCLRhE (2022).

33. J. A. Navarro et al., "Integration of UAV, sentinel-1, and sentinel-2 data for mangrove plantation aboveground biomass monitoring in Senegal," *Remote Sens.* **11**(1), 77 (2019).

34. C. E. Akumu, E. O. Amadi, and S. Dennis, "Application of drone and WorldView-4 satellite data in mapping and monitoring grazing land cover and pasture quality: pre- and post-flooding," *Land* **10**(3), 321 (2021).

35. M. Sozzi et al., "Comparing vineyard imagery acquired from Sentinel-2 and unmanned aerial vehicle (UAV) platform," *OENO One* **54**(2), 189–197 (2020).

36. L. Kuşak et al., "Modelling of a landslide site with satellite and UAV," in *Cilicia International Symposium on Engineering and Technology At: Mersin* (2019).

37. M. R. M. Mokhtar et al., "Assessing UAV landslide mapping using unmanned aerial vehicle (UAV) for landslide mapping activity," *Appl. Mech. Mater.* **567**, 669–674 (2014).

38. A. Alptekin et al., "Illustrating of a landslide site with photogrammetric and LIDAR methods," in *Advances in Science, Technology & Innovation*, H. El-Askary et al., eds., pp. 303–305, Springer, Cham (2022).

39. J. Qi, H. Chen, and F. Chen, "Extraction of landslide features in UAV remote sensing images based on machine vision and image enhancement technology," *Neural Comput. Appl.* **34**(15), 12283–12297 (2022).

40. H. He et al., "Multisource data fusion and adversarial nets for landslide extraction from UAV-photogrammetry-derived data," *Remote Sens.* **14**(13), 3059 (2022).

41. K. Tempa et al., "UAV technique to localize landslide susceptibility and mitigation proposal: a case of Rinchending Goenpa landslide in Bhutan," *Nat. Hazards Res.* **1**(4), 171–186 (2021).

42. P. C. Pesántez, "Land movement detection from UAV images," *Int. Arch. Photogramm. Remote Sens. Sp. Inf. Sci.* **XLIII-B2-2**, 1071–1076 (2022).

43. R. Pati, K. Rajesh, and D. Kanungo, "Application of UAV for landslide mapping, modelling and monitoring," in *Proc. Int. Conf. EGCON - 2021* (2021).

44. J. C. Padró et al., "Radiometric correction of landsat-8 and sentinel-2A scenes using drone imagery in synergy with field spectroradiometry," *Remote Sens.* **10**(11), 1687 (2018).

45. S. Zhang et al., "Integrated satellite, unmanned aerial vehicle (UAV) and ground inversion of the SPAD of winter wheat in the reviving stage," *Sensors* **19**(7), 1485 (2019).

46. M. Pla et al., "Calibrating sentinel-2 imagery with multispectral UAV derived information to quantify damages in mediterranean rice crops caused by western Swamphen (Porphyrio porphyrio)," *Drones* **3**(2), 45 (2019).

47. A. Revill et al., "Quantifying uncertainty and bridging the scaling gap in the retrieval of leaf area index by coupling sentinel-2 and UAV observations," *Remote Sens.* **12**(11), 1843 (2020).

48. X. Guo et al., "Estimating mangrove leaf area index based on red-edge vegetation indices: a comparison among UAV, WorldView-2 and Sentinel-2 imagery," *Int. J. Appl. Earth Observ. Geoinf.* **103**, 102493 (2021).

49. T. Gränzig et al., "Mapping the fractional coverage of the invasive shrub Ulex europaeus with multi-temporal Sentinel-2 imagery utilizing UAV orthoimages and a new spatial optimization approach," *Int. J. Appl. Earth Observ. Geoinf.* **96**, 102281 (2021).

50. S. Thapa, V. E. Garcia Millan, and L. Eklundh, "Assessing forest phenology: a multi-scale comparison of near-surface (UAV, spectral reflectance sensor, PhenoCam) and satellite (MODIS, Sentinel-2) remote sensing," *Remote Sens.* **13**(8), 1597 (2021).

51. A. Daryaei et al., "Fine-scale detection of vegetation in semi-arid mountainous areas with focus on riparian landscapes using Sentinel-2 and UAV data," *Comput. Electron. Agric.* **177**, 105686 (2020).

52. J. Jiang et al., "Multi-sensor and multi-platform consistency and interoperability between UAV, Planet CubeSat, Sentinel-2, and Landsat reflectance data," *GISci. Remote Sens.* **59**(1), 936–958 (2022).

53. D. Moravec et al., "Effect of atmospheric corrections on NDVI: intercomparability of Landsat 8, Sentinel-2, and UAV Sensors," *Remote Sens.* **13**(18), 3550 (2021).

54. "Early warning portal of KG," https://sropasture.kg/ (accessed 12 May 2022).

55. "Agisoft Metashape: Installer," 2022, https://www.agisoft.com/downloads/installer/ (accessed 6 September 2022).

56. F. N. Kogan, "Application of vegetation index and brightness temperature for drought detection," *Adv. Sp. Res.* **15**(11), 91–100 (1995).

57. M. Svoboda and B. A. Fuchs, *Handbook of Drought Indicators and Indices*, World Meteorological Organization, Geneva (2016).

58. M. Kulikov and U. Schickhoff, "Vegetation and climate interaction patterns in Kyrgyzstan: spatial discretization based on time series analysis," *Erdkunde* **71**(2), 143–165 (2017).

59. N. P. Nezlin, A. G. Kostianoy, and B. L. Li, "Inter-annual variability and interaction of remote-sensed vegetation index and atmospheric precipitation in the Aral Sea region," *J. Arid Environ.* **62**(4), 677–700 (2005).

60. P. A. Propastin et al., "Remote sensing based study on intra-annual dynamics of vegetation and climate in drylands of Kazakhastan," *Basic Appl. Dryland Res.* **1**(2), 138–154 (2007).

61. U. Gessner et al., "The relationship between precipitation anomalies and satellite-derived vegetation activity in Central Asia," *Glob. Planet. Change* **110**, 74–87 (2013).

Erkin Isaev received his diploma degree in hydrometeorology from the Russian State Hydrometeorological University in 2014 and his PhD in meteorology, agrometeorology, and climatology from the same university in 2017. He is a research fellow at the Mountain Societies Research Institute (MSRI) of the University of Central Asia (UCA). His current research interests include remote sensing, meteorology, natural hazards, dynamics and physics of the atmosphere, air pollution, and modeling and predictive analysis using machine learning (ML).

Maksim Kulikov received his BSc degree in information systems from Kyrgyz State Technical University, his MSc degree in environmental management from the International University of Kyrgyzstan, and his PhD in excellence in geography and natural sciences from the Institute of Geography, University of Hamburg, Germany. He is a research fellow at the MSRI of the UCA. His current research interests include soil, vegetation, as well as remote sensing, geographic information system (GIS), and modeling of natural ecosystem processes.

Evgenii Shibkov received his bachelor's degree in world economy from the Faculty of International Relations, Kyrgyz-Russian Slavic University, Bishkek, Kyrgyzstan, and his MS degree in geomarketing, geodata modeling, and cartography in 2014 from Kyrgyz State University of Construction, Transport, and Architecture. He is a research associate at the MSRI of the UCA. His current research interests include forest, pasture, and water resources management, including GIS and remote sensing applications.

Roy C. Sidle is a director of the MSRI and a professor of the Earth and Environmental Sciences at UCA. His interests include hydrological processes, climate change impacts, natural hazards, cryosphere, land degradation, and food security. He has more than 220 publications in journals and more than 300 book chapters. These works have been cited more than 16,500 times. He was elected as a fellow in AGU (2010), received the international award from the Japan Society of Hydrology and Water Resources (2014), and presented the hydrological sciences distinguished lecture at the 2017 Asia Oceania Geosciences Society meeting.